Burning Behavior of ADN-Based Propellants Loaded with Al-Mg Mechanically Activated Powders

F. Cristilli[1,2], V. Weiser[1], F. Maggi[2], A. Imiolek[1], C. Tagliabue[1], V. Gettwert[1], and S. Dossi[2]*

*Corresponding Author volker.weiser@ict.fraunhofer.de

[1]*Fraunhofer Institute for Chemical Technology, Joseph-von-Fraunhofer-Str. 7, 76327 Pfinztal, Germany*

[2]*Politecnico di Milano, Dept. of Aerospace Science and Technology,*

Via La Masa 34, 20156 Milan, Italy

Abstract

The experimental study presented in this paper aims at investigating the influence of mechanically activated Al-Mg powders on the burning behavior of ADN-based composite propellants. Three different powders were employed: a non-treated blend of Al and Mg and two others batches produced with different intensities of the activation process. As binder, hydroxyl-terminated polybutadiene (HTPB) was used, with and without the metal fuel.

The propellants were tested in a window bomb pressurized by nitrogen. The burning rate was measured over a pressure range from 4 to 13 MPa using a digital high-speed video camera. The temperatures of the hot gases and particles were derived from the emission spectra in the UV/Vis/NIR range. Along with the burning behavior and the powders characterization, the agglomeration phenomena are also discussed.

The investigated propellants featured a pressure exponent ranging from 0.65 to 0.87, with a relatively low flame temperature. The results have evidenced that the influence of the Al-Mg mixture cannot be correlated to that of the individual metals, while the activation treatment exerts a strong effect on the propellants ballistics.

1. Introduction

In recent years, it has taken a great awareness of the risks associated with the use of ammonium perchlorate and the research community has turned attention to new alternatives that may offer the same performance while still being environmentally friendly. On paper, ammonium dinitramide appears as the best candidate: density, oxygen balance, and an excellent enthalpy of formation. Besides being an attractive oxidizer from the energetic viewpoint, the dinitramide anion is halogen-free, thus assuring a minimal environmental and health impact. In addition, the absence of chlorine makes ADN desirable for smokeless propellants.

Several studies have been conducted on the burning behavior of ADN-based propellants and a brief review is proposed hereinafter, focusing on inert binders (Table 1). Specific attention was paid to "pure formulations" i.e. those without any additives or other oxidizers than ADN in order to draw the most generic considerations. In essence, it turns out that ADN, coupled with an inert binder, suffers from having a very high pressure exponent, way above the values of practical interest for space applications. Besides safety concerns, a high pressure sensitivity is to be avoided in order to limit the influence of pressure fluctuations on the propellant ballistics. Indeed, in most rocket motors the exponent lies in the range between 0.2 and 0.6. Considering that for launch vehicles the typical burning rate is around 7 and/to 15 mm/s at 7 MPa, the HTPB/ADN couple succeeds in meeting this requirement, however the ballistic exponent remains the main hindrance and appears to be a common feature of all inert polymers in combination with ADN.

Such behavior might be correlated with the combustion mechanism of ADN and how the decomposition products from both the oxidizer and the binder interact with each other. Parr *et al.* [1][2] investigated the flame structure of ADN sandwiches with a number of energetic and inert binders at low pressures, using planar laser-induced fluorescence (PLIF) imaging. Diffusion flames were found but their standoff distance was too high to exert any significant influence on the burning rate. Since the pressure dependence of ADN is strongly altered when an inert binder is added, there could be an intense interaction between the two. Given that at low pressure the diffusion flames place themselves far from the burning surface, as pressure increases the augmented reaction kinetics causes

the flame front to approach the burning surface, thus enhancing its importance. This phenomenon could explain the high pressure sensitivity exhibited by this class of propellants, as hypothesized in [3][4].

Table 1: Literature review of the ballistic properties of ADN coupled with an inert binder.

Formulation			Ballistic Properties			Ref.
Binder (wt. %)	Oxidizer (size) (wt. %)	Metal (size) (wt. %)	a $(mm/s)/(MPa)^n$	n (-)	r_{b7} (mm/s)	
HTPB 25	ADN (187 µm) 60	Al (13.2 µm) 15	2.5 ± 0.3	0.87 ± 0.04	13.6[a]	[5]
HTPB 25	ADN (187 µm) 60	Al (30.0 µm) 15	2.4 ± 0.3	0.87 ± 0.04	13.1[a]	
HTPB 20	ADN (187 µm) 64	Al (13.2 µm) 16	2.5 ± 0.4	0.91 ± 0.07	14.7[a]	
HTPB 30	ADN (99 – 300 µm)[b] 70	none 0	-	1.1	-	[6]
TPE[c] 30	ADN (raw crystals) 70	none 0	-	2.7	-	
TPE[c] 20	ADN (raw crystals) 80	none 0	-	1.0	-	
TPE[c] 10	ADN (raw crystals) 90	none 0	-	0.7	-	
PCL[d] 10	ADN (40 µm) 80	Al (15 µm)[b] 10	-	1.0	-	[7]
PCL[d] 11	ADN (40 µm) 89	none 0	3.97	1.0	26.5[a]	
HTPB 17	ADN (48 – 212 µm) 65	Al (4 – 20 µm) 18	1.74	1.01	13.8	[8]
Desmo[e] 22	ADN (48 – 218 µm) 60	Al (4 – 20 µm) 18	1.73	1.07	14.7	

[a]Calculated from the Vielle's law.   [b]D_{43}, volume mean diameter.
[c]Thermoplastic elastomer.   [d]Polycaprolactone.
[e]Desmophen® 2200 B.

The purpose of the present work is to evaluate the influence of mechanically activated Al-Mg powders on the burning behavior of HTPB/ADN propellants. Such activated powders consist in standard micrometric powders that, after a mechanical treatment, gain an augmented reactivity. During the process, the metal particles are subjected to intense mechanical stresses that may significantly alter their morphology. The repeated impacts between the particles and the grinding spheres cause severe plastic deformations in the metal, thus promoting substantial shape, dimension and surface modifications. The treatment yields a final product with a higher specific surface, a figure of merit for the reactivity of a metal powder. The milling process opens up a number of possibilities to modify the characteristics of a powder. For instance, the reactivity can be tailored by the inclusion of additives [9][10][11] as it was done in the present study with magnesium. In consequence of the treatment, different particles (metal and additive(s)) merge together, giving rise to a composite powder. Although the magnesium is not as performing as aluminum from the energetic viewpoint, its high volatility and the permeability of its oxide favor a prompter ignition, closer to the burning surface. It is therefore believed that the enhanced reactivity provided by both the addition of magnesium and the activation treatment could bring benefit to the ballistic performance.

2. Experimental Techniques

The combustion tests were performed by using the ICT window bomb facility. The apparatus can be pressurized either by oxygen, air, argon or nitrogen, from 0.02 MPa up to 18 MPa. In the present work, the steady burning rate was measured at 4, 7, 10 and 13 MPa, whereas the agglomeration phenomena were examined in dedicated combustion tests at 4 MPa; in either case nitrogen was used to pressurize the vessel. For the burning rate

measurements, the propellant strands (5x5x30 mm) were coated with a polyurea coating (FlexCoat Rapid, Grountech) to prevent any irregular or lateral burning. Unless otherwise stated, the ignition was provided by a booster charge, in turn initiated with a nickelin fuse wire.
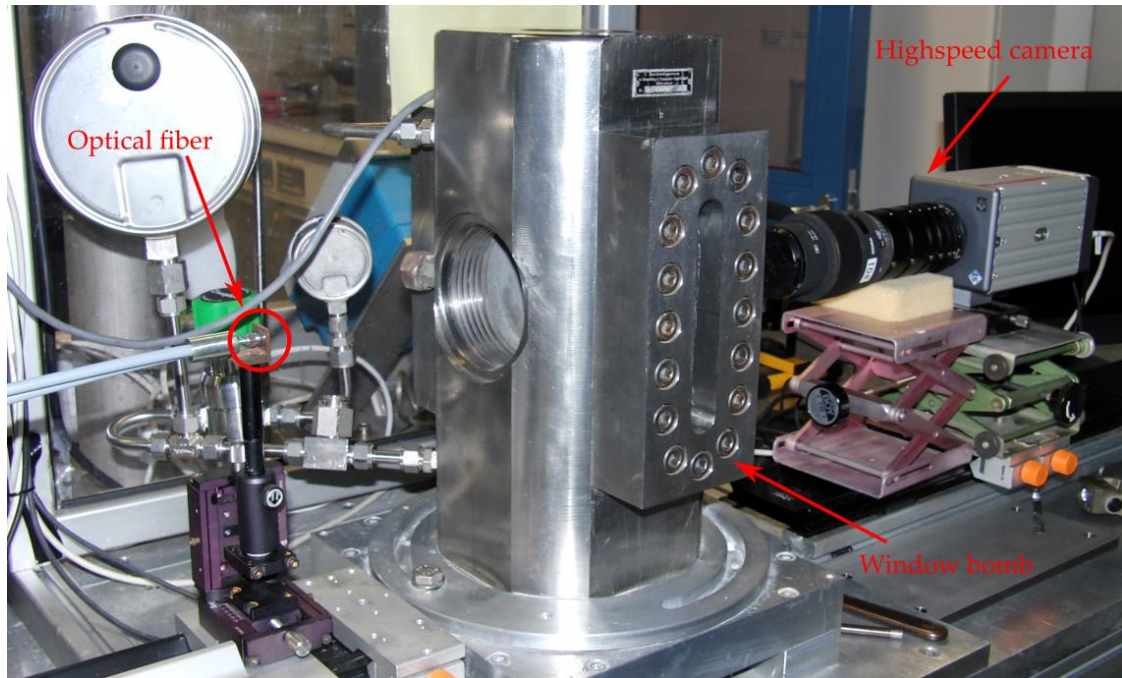

Figure 1: Experimental setup.

The bomb offers four optical accesses whose glass pane can be replaced based on need; a Crown glass window was used for videography and a quartz window was used for spectroscopic investigations. Each test was recorded with a high-speed camera, while the emission spectra from both the flame including particles were captured by a twin emission spectrometer. The whole ensemble is shown in Figure 1. To enable a clearer and smokeless visualization, the measurements were carried out under a steady flow of ∼15 kg/h.

The condensed combustion products (CCPs) from the combustion of uncoated samples were collected to get some qualitative and quantitative information about the agglomerates. The tests were performed at 4 MPa and the residues were collected by a SEM sample holder placed upside-down inside the bomb, at a fixed distance of 5 mm above the specimens' upper side. Thereafter, the products were analyzed via a scanning electron microscope.

2.1 Highspeed Camera

The burning tests were recorded with a 24 bit color high-speed camera MotionPro® X3 by Redlake. This model features a recording frequency varying from 1000 fps at full resolution (1280x1024) to 64000 fps at 1280x16, along with the possibility of having a shutter speed as low as 1 µs. For the burning rate measurements, the frame rate was adjusted according to pressure so as to obtain at least 700 frames per video. For such tests the camera was equipped with a 105 mm macro lens, thus achieving a scale factor as low as 14 µm/pixel.

2.2 Spectrometer

Solid propellants generally feature flame temperatures lying in the range from 1000 K to >3000 K, which correspond to intensity peaks spreading from the near infrared to the short wavelength infrared spectral ranges. Emission spectra from both condense materials and the gas phase were recorded with the combination of two spectrometers connected in one casing, in order to cover the wavelength range from ultraviolet to infrared. The technical specifications of the two devices are summarized in Table 2. The intensity calibration was performed by taking as reference the radiation from a black body at a given temperature. Subsequently, a corrective factor was derived from the ratio between the Planck's emission and the measured spectrum. The measurements spatial resolution was approx. 3 to 4 mm.

Table 2: MCS621 Vis2 and MCS611 NIR2.2 spectrometers, technical specifications.

	MCS621 Vis2	MCS611 NIR2.2
Detector	Hamamatsu Si diode array, 256 pixel	Hamamatsu InGaAs diode array, 256 pixel
Monochromator	Flat field, 366 lines/mm	Plan mesh, 300 lines/mm
Spectral range (nm)	$310 - 1100$	$900 - 2140$
Integration time (ms)	$3 - 5000$	$0.3 - 2000$
Reading frequency (Hz)	Max. 60	Max. 60
Spectral resolution (nm)	10	18

2.3 Burning rate

The burning rate was evaluated by means of the ICT software Video Analyzer. The latter processes each video frame by frame, and gives as output a single picture representative of the overall sequence. This allows to easily detect the presence of bright or dark flame zones, or other features that would otherwise be difficult to recognize. Once both the scale and the frame rate are given, the burning rate is derived from the slope of the line described by the regression of the burning surface, as shown in Figure 2. The more the combustion proceeds uniformly, the sharper and straighter is such "regression line", and therefore easier to identify. When this was not possible, due to an abundant smoke and/or a non-homogeneous surface regression, the test was repeated. However, the program also enables the user to select a narrower region of interest, whose burning is more even.
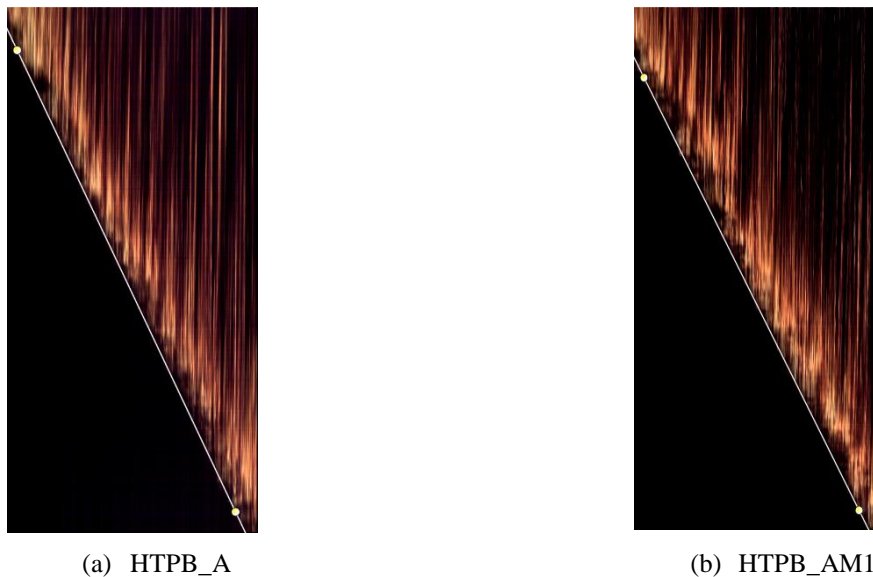

(a) HTPB_A   (b) HTPB_AM1

Figure 2: Examples of regression lines from different propellants.

2.4 Temperature

The spectra were analyzed via the ICT-BaM software. Basing on tabulated data [12] and theoretical models, the program is able to calculate the NIR/IR spectra of many chemical species, including H_2O, CO_2, CO, NO, HCl as well as soot particles. Under the hypothesis of a homogeneous flame, the temperatures were evaluated by a least squares fitting between the calculated and the measured spectra, using the temperature itself and the concentrations of the species as parameters. The temperature of the hot solid particles was derived from the continuum radiation according to the gray body model, whereas the gas phase temperature was obtained from the water bands. A more detailed picture of the process is described elsewhere [13].

2.5 Additional Analyses

Supplementary analyses were carried out to characterize the activated powders and examine the condensed combustion products. The instruments are summarized in Table 3.

Table 3: Instruments employed for additional analyses.

Analysis	Instrument
SEM/EDX	Zeiss Supra VP 55
TG/DSC	NETZSCH STA 449 C
XRD	D8 Bruker AXS
Heat of Combustion	IKA C2000
Particle Size	Malvern Mastersizer 2000
Specific Surface	Quantachrome NOVA 2000e

3. Investigated Formulations

Two distinct sets of propellants were produced and investigated, as summarized in Table 4. The HTPB series was loaded with three different Al-Mg powders, while the aluminized formulation (HTPB_A) was used as benchmark. The metal powders were labeled by a specific nomenclature, as described in Table 5. The binder content was imposed by processability constrains, while the metal/oxidizer ratio was chosen basing on the theoretical maximum specific impulse at 7 MPa, calculated under the hypothesis of adapted equilibrium at sea level. The thermochemical calculations were performed by using the ICT-Thermodynamic Code [14].

These formulations were conceived with the aim of probing the influence of both the addition of magnesium and the activation process. Differently, the HADN series was tested to get a better understanding of the effect of the two separated metals with respect to the non-metalized propellant. The composition was chosen as follows: the metal amount was set as the corresponding "HTPB" propellants, while the oxidizer/binder mass ratio was kept fixed, equal to the non metalized formulation.

Table 4: Investigated formulations.

Propellant ID	Binder (wt. %)	Oxidizer (wt. %)	Metal (wt. %)
HTPB-Series			Al (16)
HTPB_A			
HTPB_AM0	HTPB[a] (18)	ADN[b] (66)	AM0 (16)
HTPB_AM1			AM1 (16)
HTPB_AM2			AM2 (16)
HADN-Series			Al (16)
HADN_A	HTPB (20)	ADN (64)	
HADN_M			Mg (16)
HADN	HTPB (24)	ADN (76)	-

[a] Polyvest® EP HT by Evonik Industries AG.

[b] 176 μm prills by Eurenco.

The propellant slurries were prepared by using the planetary centrifugal kneader THINKY MIXER ARV-310 by THINKY. The device is designed for handling a relatively small amount of material, but enabling a very fast operation. The process can be performed under vacuum, and the mixing is realized by both rotation and revolution movements, without employing any blade. On the other hand, the temperature cannot be directly controlled. The ingredients were added one at a time, adjusting the rotational speed (1400 - 2000 rpm) accordingly, in order to keep the temperature always below 40 °C. Isophorone diisocyanate (IPDI) was used as curing agent.

The mixing process was performed under vacuum (p $\sim$ 10 mbar) to remove any air bubbles. Additionally, the metal powders were dried under vacuum for 24 hours, prior to use. The propellant slurries were then cast in the molds, previously pre-heated at 40 °C. Finally, the propellants were cured for seven days at 40 °C.

Table 5: Nomenclature adopted for the metal powders.

Label	Powder	Description
_A	Aluminum particles (15 µm)	Supplied by Avio S.P.A.
_M	Magnesium flakes (325 mesh size)	Prod. by Alfa Aesar GmbH & Co KG
_AM0	Al-Mg mixture (80 – 20 wt. %)	Not treated
_AM1	Al-Mg mixture (80 – 20 wt. %)	Low mechanical activation
_AM2	Al-Mg mixture (80 – 20 wt. %)	Intense mechanical activation

The activated powders were produced at the Space Propulsion Laboratory (SPLab) of the Polytechnic University of Milan. The activation was achieved by employing the planetary ball mill PM 100 by Retsch. The mill enables to accurately control the grinding time and the rotational regime, which can be also set to operate in an alternate clockwise-counterclockwise mode. Once that the milling parameters are selected, the powder is inserted into the grinding jar along with the steel spheres, according to the ball-to-powder ratio (BPR) chosen. By changing settings of the process one can get different levels of activation, as it was done with the powders AM1 and AM2. A process controlling agent (PCA) was used to avoid cold welding between the particles. Both the jar and the spheres were carefully cleaned after every usage.

4. Results and Discussion

The present section is dedicated to the presentation and the discussion of the experimental results. The characterization of the activated powders is reported first, then the results from the combustion tests follow.

4.1 Powder Characterization

The Al-Mg powders AM0, AM1 and AM2 were extensively characterized in order to assess the effects of the activation process in comparison with the untreated powder AM0.

SEM pictures are reported in Figure 4. In the AM0 powder it is clear to recognize the aluminum particles - spherical - from the magnesium flakes, which are additionally slightly more irregular in their surface texture. On the contrary, the morphology of the activated powders was strongly altered by the process and it is therefore difficult to distinguish the metals. The surface appears more uneven, indented by rough edges. The low-activated powder AM1 is mainly composed by flakes of various dimensions, while AM2 features more rounded, yet not spherical, particles, as though they originated from different flakes clumped together. The smaller elements, below ~ 10 µm, are composed by either tiny shards or almost untouched particles, thus evidencing the difficulty of treating very small parts. Figure 5 shows two pictures obtained through EDX mapping. The most activated power - AM2 - exhibits a more homogeneous dispersion of the ingredients, with the presence of small magnesium fragments (red) embedded in the aluminum (green). It is believed that such intimate mixing could precipitate the Al ignition thanks to the local heating provided by the oxidation of Mg.
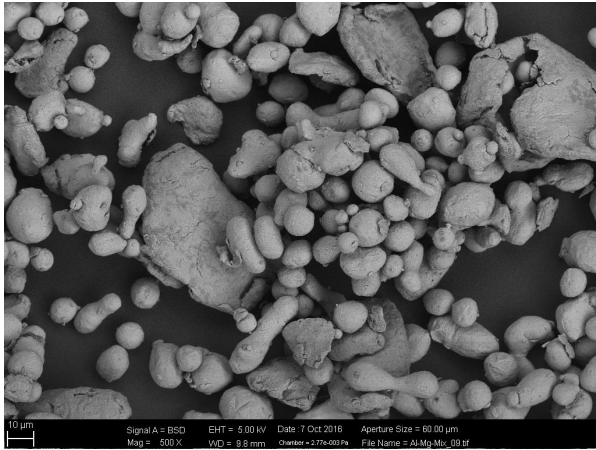
Figure 6 shows the particle size distributions, measured via laser granulometry. It is worthy specifying that, given the powders irregular morphology, the results obtained with this technique are not valid on an absolute scale, but rather allow to highlight the differences between the samples. As the intensity of the milling process increases, the size distribution shifts towards higher values. The powder AM1 has a marked shoulder, a sign that it was not homogeneously altered - in size - but some particles were ground more than others. It is therefore possible that this could have effects on the burning behavior of the propellants. The AM2, being more activated, features a more uniform distribution. The main parameters that describe the distributions are summarized in Table 6. D(0.1) and D(0.9) represent the 10th and the 90th percentiles, while the span is a measure of the data spreading.

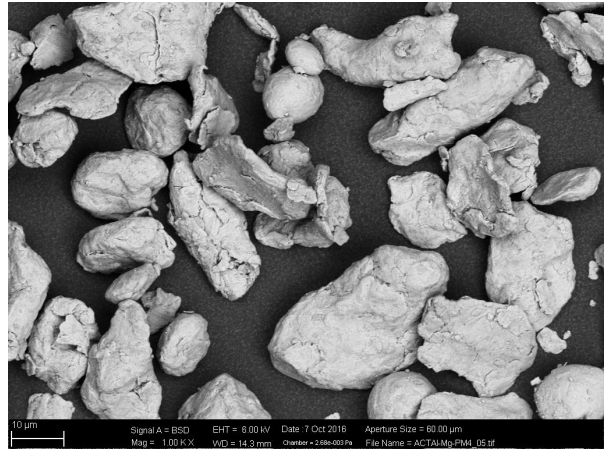Table 6: Size distribution parameters for the Al-Mg powders.

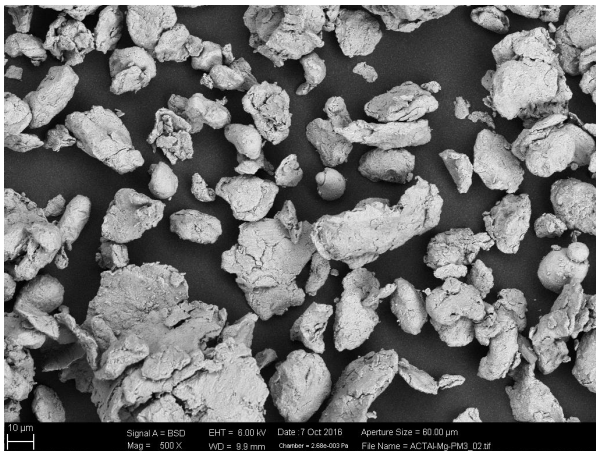| Powder	D[1,0]	D[3,2]	D[4,3]	D(0.1)	D(0.9)	Span[a]
AM0	22.30 ± 0.08	19.55 ± 0.05	27.78 ± 0.13	10.79 ± 0.01	52.53 ± 1.07	1.89 ± 0.01
AM1	28.42 ± 0.27	24.21 ± 0.19	48.31 ± 1.32	12.02 ± 0.03	118.81 ± 4.66	3.76 ± 0.13
AM2	37.32 ± 0.27	29.57 ± 0.16	52.48 ± 0.99	14.44 ± 0.04	114.50 ± 2.27	2.68 ± 0.04

[a]Span = (D(0.9) – D(0.1))/D(0.5)
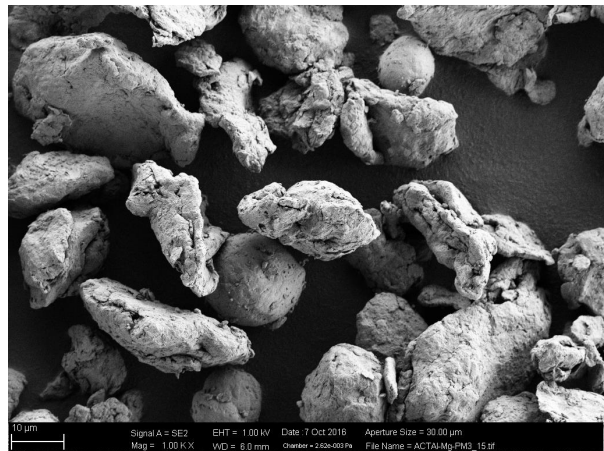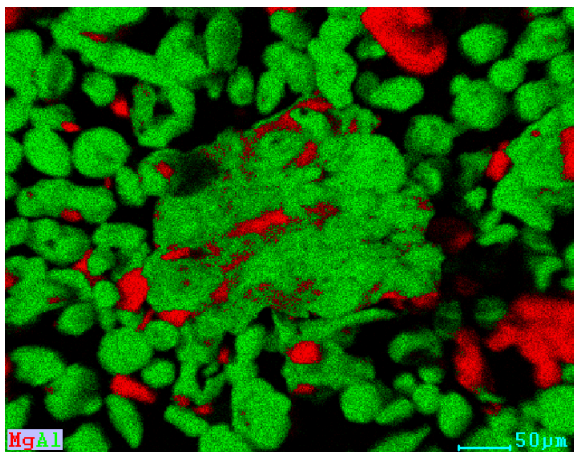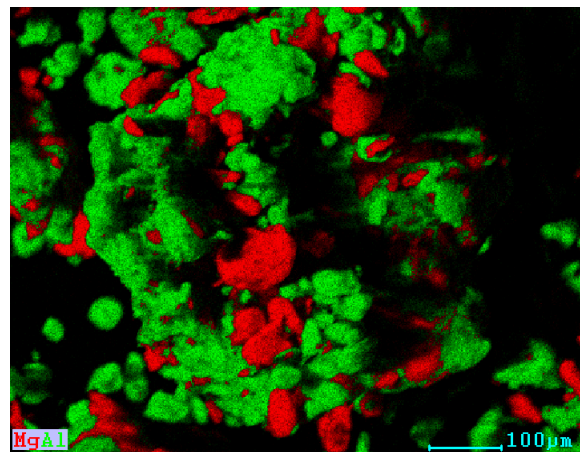
(a) AM0

(b) AM1

(c) AM2

Figure 1: SEM pictures of the Al-Mg powder at various magnifications.

(a) AM1

(b) AM2

Figure 2: EDX mapping: AM1 (left) and AM2 (right). Al and Mg are indicated by green and red respectively.
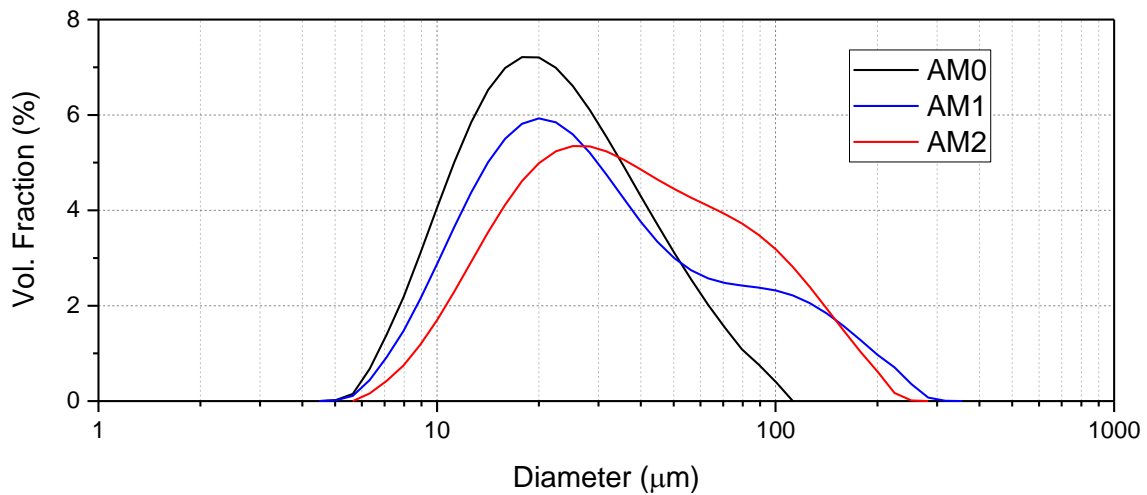
Figure 6: Particle size distributions of the Al-Mg powders.

The powders were analyzed by X-Ray Diffraction (XRD) to ascertain if any Al-Mg alloy was formed during the milling process; indeed, the presence of magnalium was strongly unwanted since it has a lower heat of combustion as compared to the individual components. In addition, a secondary purpose was to find out whether the crystalline structure was altered by the treatment. The spectra are shown in Figure 7. The measured peaks perfectly match the diffraction patterns of the pure elements and no significant difference between the samples was appreciated. The noisy continuum is ascribed to aluminum oxide, amorphous at ambient temperature. It is therefore concluded that the activation had an effect only on the macroscale, and no alloy was formed.
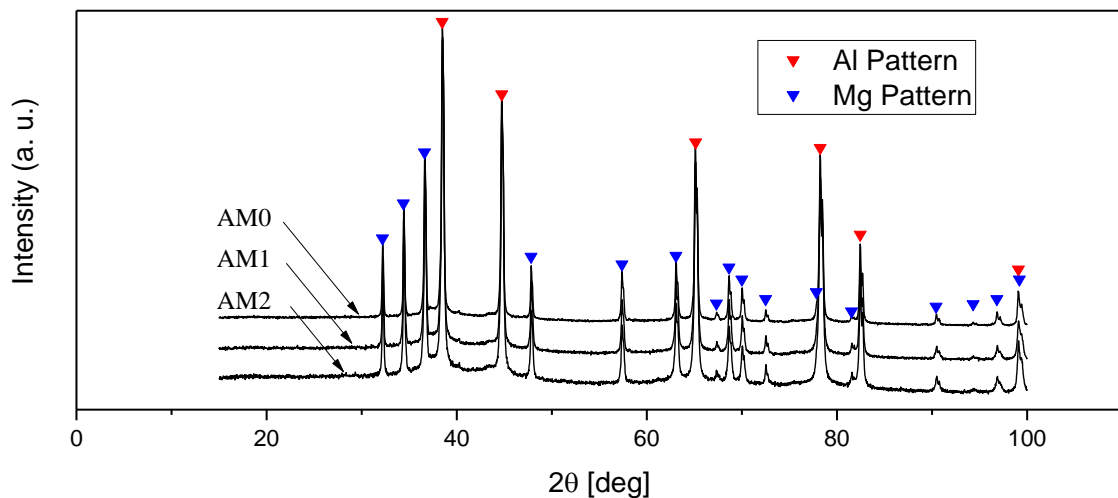

Figure 7: XRD spectra of the Al-Mg powders.

The powders were tested by means of non-isothermal oxidation in pure oxygen, from ambient temperature up to 1850 K. Figure 8 depicts the TG trace obtained under a heating rate of 10 K/min. After an imperceptible mass loss due to the desorption of gases ($\sim$ 0.2 wt. %), three main oxidation steps were identified: the first between 750 and 1000 K, the second from 1000 to 1200 K and finally the third above 1200 K. For each stage, both the onset temperature and the mass gain were derived (Table 7). The onset temperatures were calculated from the intersection of the tangents to two consecutive inflection points (local minima and maxima of the TG first derivative). The mass increase related to each oxidation step was evaluated at the corresponding inflection point (local minima). The effectiveness of the activation was proven by the shift of the onset temperatures, especially the first one; a powder with a high specific surface can benefit from an enhanced reactivity and therefore gets oxidized to a greater extent. However, the curves do not only shift, but they also change in shape, as for AM2. It follows that, for what may concern the thermal analysis, an intense treatment can noticeably modify the nature of a powder.
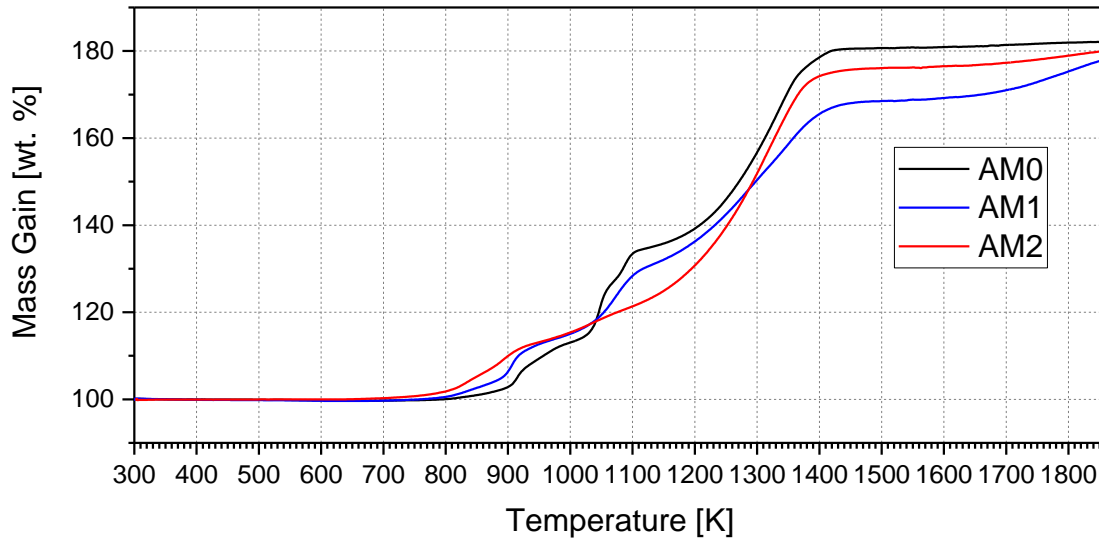
8

Figure 8: TG traces of the Al-Mg powders. The measurements were performed in pure oxygen at 10K/min.

The first oxidation step can be ascribed to magnesium oxidation only, whose theoretical contribution to the overall mass gain is 13.17 wt. %. The second stage becomes less important from AM0 to AM2, whereas the third gets more prominent. The overall mass gain is limited by the active content which typically decreases during the milling due to the exposure of the metal core to the external environment in consequence of the severe stresses and deformations.

Table 7: Reactivity parameters derived from the thermogravimetric analyses at 10K/min.

Powder	Onset Temperature (K)			Mass Gain (wt. %)		
	I	II	III	I	II	III
AM0	883 ± 3	1031 ± 2	1240 ± 4	13.32 ± 0.82	21.82 ± 2.26	46.89 ± 1.92
AM1	826 ± 6	1036 ± 13	1210 ± 6	14.10 ± 0.19	17.45 ± 1.40	46.70 ± 0.19
AM2	789 ± 32	991 ± 44	1218 ± 1	13.00 ± 1.01	7.05 ± 5.40	59.42 ± 2.41

The results from additional measurements are reported in Table 8. The specific surface - S_{sp} - was calculated according to the BET model from the isothermal adsorption of N_2 molecules. By recalling what has been already mentioned, one of the main results from an activation process is the gain in the specific surface.

The overall active content was derived from the thermogravimetric measurements. The theoretical mass gain (84.33 wt. %) was calculated with the hypothesis that the two metals contribute in proportion to their relative mass fraction. As already addressed, the addition of magnesium goes to the detriment of the heat of combustion, which is reduced from 31.05 kJ/g of pure aluminum [15] to 29.79 kJ/g. The activated powders feature a slightly lower value than the virgin sample because of the active content.

The average size of the crystalline grains was measured from the diffraction spectra with the TOPAS software, developed by Bruker. With increasing milling intensity the grains become smaller due to the intense deformation, however the material hardens with the process and therefore the difference among the activated powders is not as steep as compared with the virgin one [16].

Table 8: Characteristics of the tested powders.

Powder	S_{sp} (m^2/g)	Active Content (wt. %)	Heat of Combustion (J/g)	Grain Size (nm)	
				Al	Mg
AM0	< 0.1	97.53 ± 1.41	28644 ± 93	127	98
AM1	0.334	95.35 ± 1.52	28083 ± 248	104	87
AM2	0.543	94.21 ± 0.51	27750 ± 50	103	74

4.2 HTPB/ADN-Based Propellants

The pressure deflagration limit (PDL) of all HTPB-based propellants was measured to lie in the range between 2 and 3 MPa. Close to the PDL a flickering flame was observed. Some magnesium-containing samples were successfully ignited at pressures as low as 2 MPa, but they were not able to sustain a stable combustion and self-extinguished shortly after the ignition. As a rule, over the entire pressure range all HTPB-ADN formulations exhibited an uneven regression of the burning surface, regardless of the inhibitory coating.

HTPB Series.   Without any exception, every formulation showed a rather dim flame, very irregular in its length and brightness. Such behavior did not attenuate with increasing pressure, and much more smoke was released upon binder decomposition. At high pressures, above 10 MPa, the burning agglomerates were clearly visible as isolated bright spots, while they were barely noticeable at lower pressures. This trait was observed to be more pronounced for the HTPB_A formulation. Moreover, the latter propellant featured a stronger tendency to form more irregular carbonaceous structures than the other magnesium-containing counterparts.

The results from the burning rate tests are shown in Figure 9, along with the regression curve represented by the solid line. The HTPB/ADN/Al formulation exhibits the higher burning rate over a wide pressure range, exceeded at elevated pressures only by the HTPB/ADN/AM1 composition due to its considerable pressure sensitivity. The propellant loaded with the non-activated aluminum-magnesium powder features almost the same burning rate law as the HTPB_A formulation, just slightly shifted towards lower values. The most activated powder - AM2 - further reduces the burning rate and faintly increases the pressure exponent. The HTPB_AM1 propellant behaves like HTPB_AM2 at lower pressures, while it tends to HTPB_AM0 and HTPB_A as the pressure increases. That said, it appears that the burning rate is essentially unaffected by the addition of magnesium, while the activation process plays a greater influence.
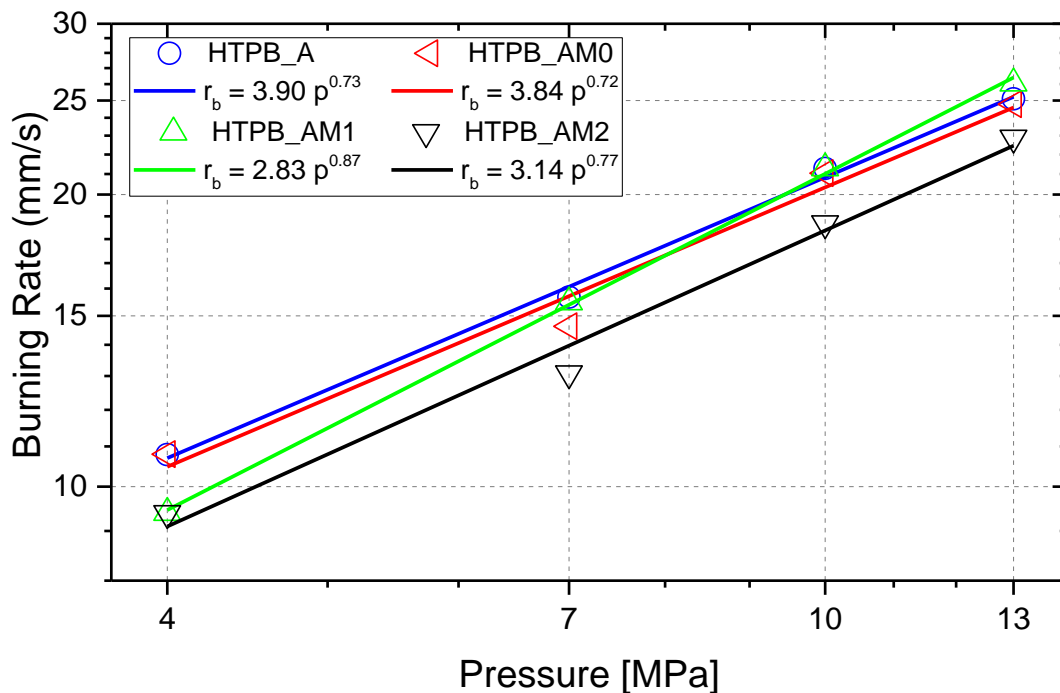

Figure 9: Burning rates of the HTPB series.

The correlation parameters, i.e. the Vielle's law coefficients, are summarized in Table 9, where the R-squared value is also reported. The burning rate at 7 MPa was taken as a reference to compare the performance of the investigated formulations. By recalling what has been already mentioned, ADN yields a very high pressure exponent when used in combination with an inert binder, and the outcomes seem to adduce an additional evidence of such characteristic. However, the present results are more promising as compared to the values reported in the open literature. Moreover, it is believed that there might be a further improvement with the addition of a ballistic modifier.

In most cases the water concentration was small and the continuum emission dominated the spectrum and made a fitting of the water spectrum impossible. Therefore only the continuum temperature related to the particles carried by the flame gases was derived. The temperature trace commonly features the highest value upon ignition. Then it exhibits a slight decreasing trend until reaching an almost steady value, whose timespan denotes the flame length. The end of the flame zone can be recognized by the abrupt temperature drop that follows the complete burnout of the metal particles. Figure 10 shows the temperature profile over the distance from the burning surface.
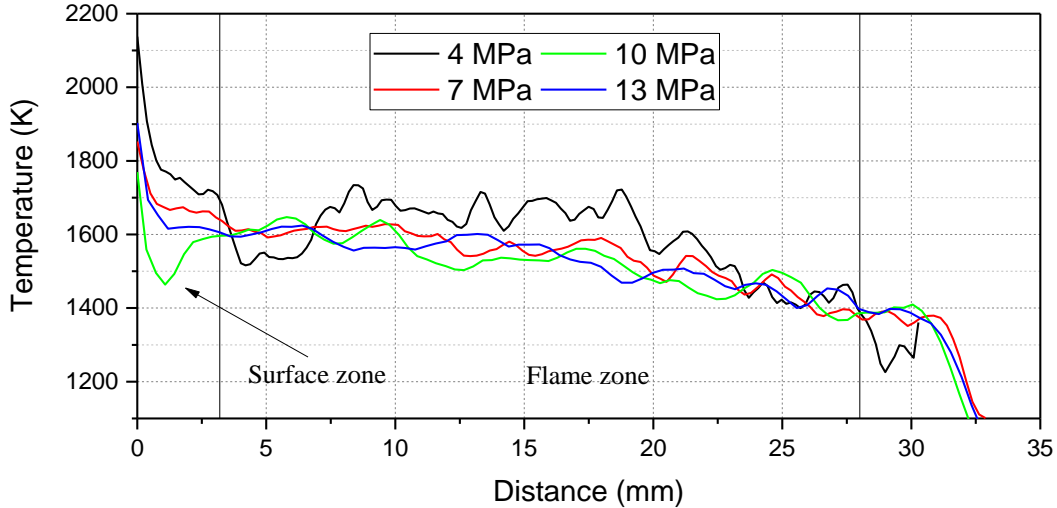

Figure 10: Spatial profile of the continuum temperature from HTPB_A at various pressures.

The curves were mildly smoothed in order to enable a clearer visualization. From the temperature time-history, the burning surface was chosen to coincide with the first peak in the emission intensity trace, which in turn corresponds to the ignition stage. Then, the distance was inferred from the time domain through the burning rate.

It turns out that the temperature profile does not vary significantly with pressure, except for some more marked fluctuations at low pressure. Likewise, the extent of the flame zone remains substantially unchanged. It is believed that the metal gets strongly oxidized very close to the surface, where the temperature is higher. While the particles detach and are carried away, they keep burning in the flame region and finally cool down rapidly as soon as the exothermic reactions stop.

Figure 11 shows the continuum temperatures from the HTPB series, calculated as the average value along the flame zone. It is worthy to notice that the absolute temperatures of the particles in the flame zone are far below the adiabatic values of the propellant formulation, which amount to about 2900 K and 2800 K for HTPB_A and HTPB_AM0/1/2. As a rule, an aluminum particle that burns in the vapor phase should have a surface temperature between the melting point of the oxide and the boiling of the metal, 2326 K and 2792 K respectively. This might be a hint to the fact that the particles were substantially oxidized close to the propellant surface and only burn out inside the flame zone with reduced intensity driven by diffusion processes inside the particles that still contain liquid metallic residual content.

On the other hand, the condensed residues that were collected (see the next section) were all spherical regardless of the morphology of the loaded powder, sign of the fact that there had been an inflammation, i.e. the onset of the homogeneous burning mode. The reasons behind such behavior are yet to be cleared, but it is a common feature of all the HTPB/ADN formulations that were tested.
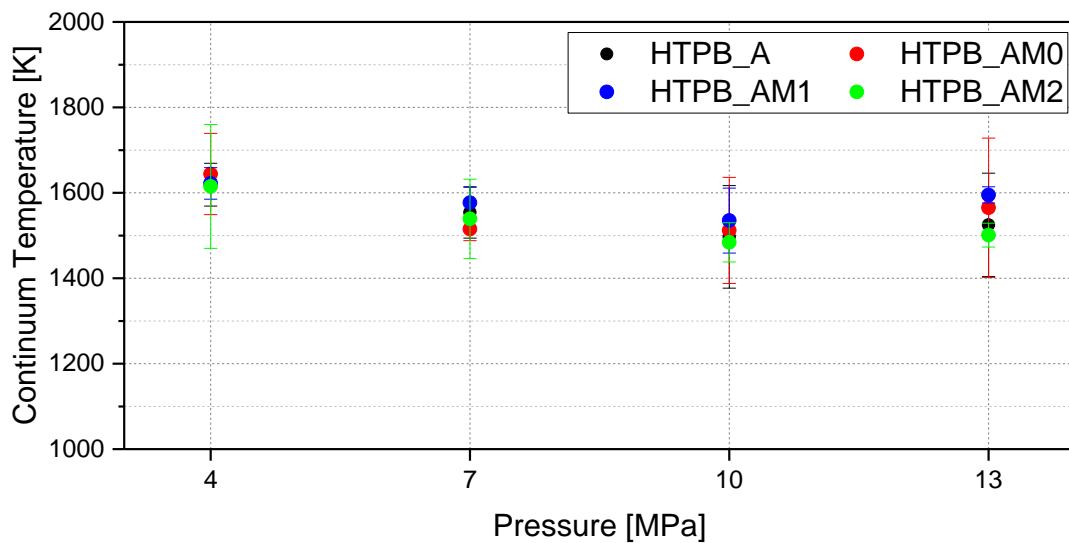
Figure 11: Continuum temperatures from the HTPB series.

The condensed combustion products (CCPs) from burning tests performed at 4 MPa were collected on an SEM sample holder, as previously described. By recalling the Glotov's classification [17], the CCPs can be divided into:

- Small oxide particles (SOPs), whose size is sub-micrometric. They amount to the ~ 80% by mass of CCPs [18][19], and originate from the coalescence and condensation of oxide vapors;
- Micrometric oxide particles (MOPs), resulting from the complete combustion of both agglomerates and isolated particles;
- Agglomerates, namely particles whose dimension exceeds the nominal size of the loaded metal powder. They mainly contain unburned aluminum along with its oxide, though some minor impurities coming from binder pyrolysis may be also present [20].

All these three classes are observed from SEM pictures. It is underlined that the size of the residue does not correspond to the dimension of the particles as soon as they detach from the propellant surface. Likewise, it is not easily comparable with the original particle size, because of the complex evolution and interactions involved during the combustion process.

Figure 12 shows some SEM pictures of the residues collected from the HTPB_A, HTPB_AM1 and HTPB_AM2 propellants. The aluminized formulation exhibited a prominent tendency to form large particles - sub-figure (a) - which has not been observed elsewhere (Figure 12, sub-figures (b) and (c)). Most of the particles are covered by nanometric SOPs, the latter resulting from the homogeneous combustion that follows the inflammation. Many particles, generally the smaller ones, feature the presence of one or multiple holes of various widths. It cannot be excluded that some of them might be entirely hollow. Such perforated particles were found to form in all the investigated propellants (Figure 12, sub-figures (b) and (c)). The formation mechanism of the so-called "hollow" agglomerates was investigated in detail by Babuk [21].
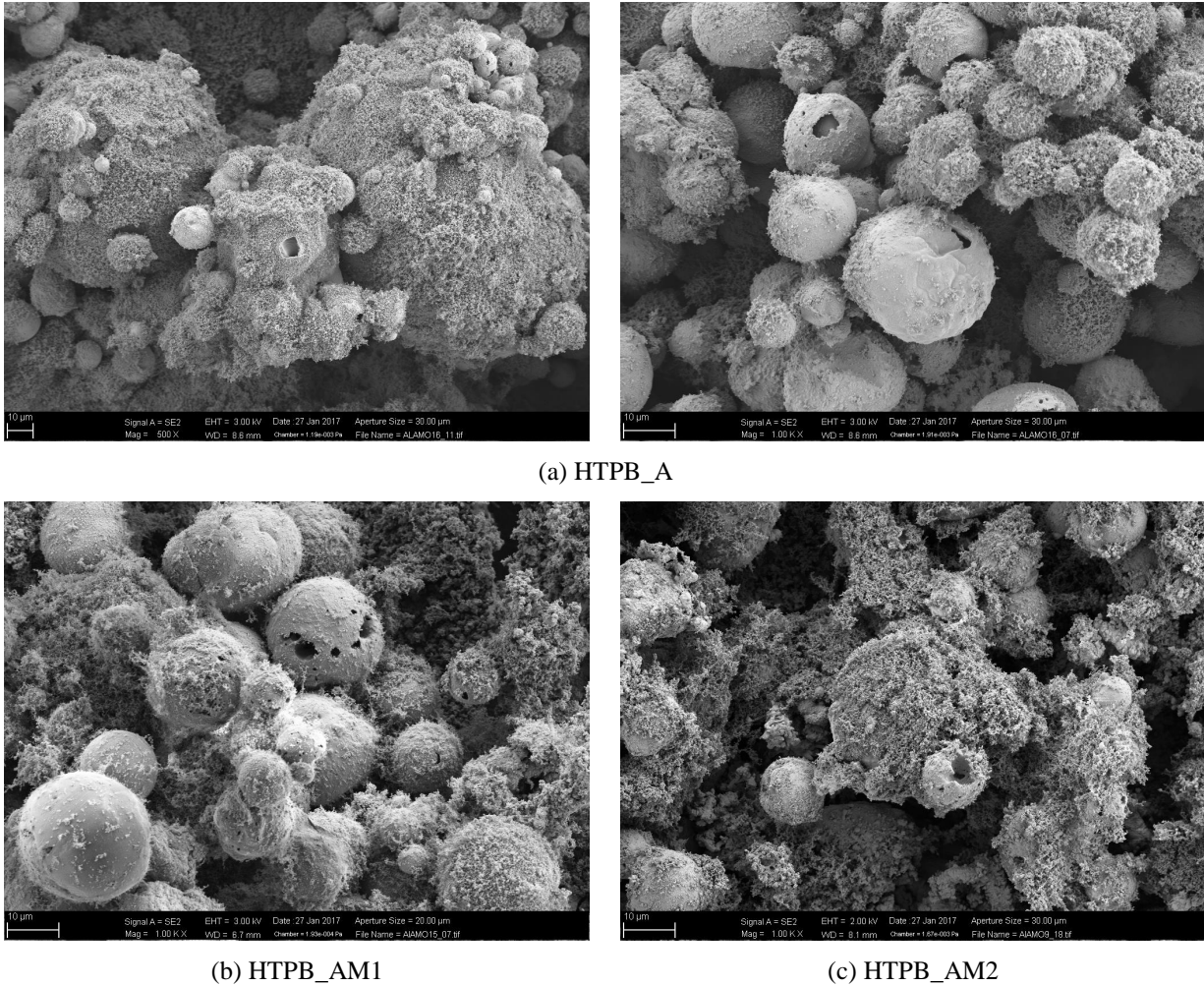
(a) HTPB_A

(b) HTPB_AM1

(c) HTPB_AM2

Figure 12: SEM pictures of the collected CCPs at various magnifications.

According to his findings, the process originates from the chemical interaction between the aluminum and its oxide at temperatures below the boiling point of the metal. Such interaction produces gaseous bubbles that eventually merge together thus forming a large cavity.

For what may concern the other formulations, the particulate is predominantly spherical, regardless of the morphology of the original powder. What remains of magnesium are essentially SOPs, which accumulate and give rise to coral-like, branched structures.

From the combustion videos, below 10 MPa no burning agglomerates are visible within the flame zone; while at higher pressure many and large glowing agglomerates were observed even above the luminous region. Such peculiar behavior can be ascribed to the temperature closed to the propellant surface that, at low pressure, could not be high enough to initiate the aggregation mechanism. It is possible that, with increasing pressure, the enhanced chemical kinetics and the greater heat feedback from the flame caused the surface temperature to exceed the Al melting point, thus giving rise to the classic agglomeration phenomenon.

HADN Series. For this series only the burning rate and the temperature were measured. The formulation containing magnesium - HADN_M - burned rather uniformly, whereas the aluminized propellant HADN_A featured a strong uneven regression.

The non-metalized formulation - HADN - exhibits the highest burning rate and the lowest pressure exponent. The addition of aluminum (HADN_A) increases the pressure sensitivity from 0.65 to 0.72, while reducing the overall burning rate. The propellant containing magnesium - HADN_M – features a similar ballistic law, with a higher exponent. By comparing HTPB_A with HADN_A it results that increasing the binder content from 18 % to 20 % does not affect the pressure exponent, whereas the pre-exponential coefficient is reduced. The results clearly show that the addition of a metal fuel reduces the burning rate, as if it contributes to the overall thermal balance as a heat sink.
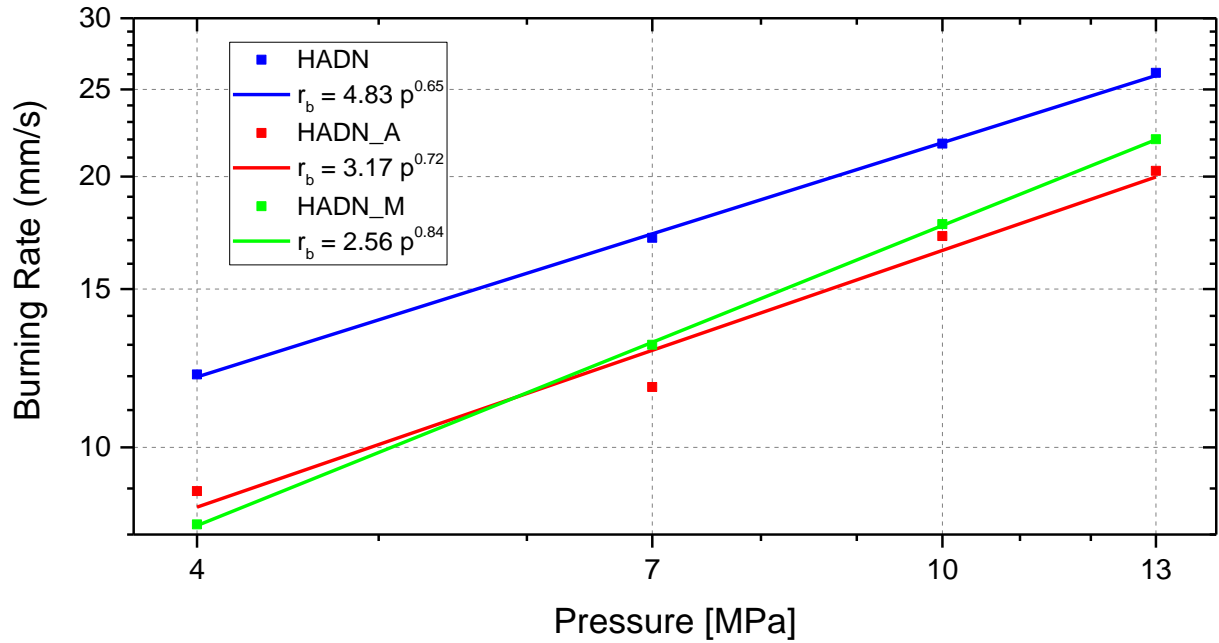
13

Figure 13: Burning rates of the HADN series.

Table 9: Vielle's law parameters ($r_b = ap^n$) for both the HTPB and HADN series. R^2 denotes the coefficient of determination of the regression curve.

Propellant ID	Ballistic Properties			R^2
	a	n	r_{b7}	
	$(mm/s)/(MPa)^n$	(-)	(mm/s)	(-)
HTPB_A	3.90 ± 0.97	0.73 ± 0.12	15.68 ± 0.58	0.9972
HTPB_AM0	3.84 ± 2.51	0.72 ± 0.29	14.63 ± 1.40	0.9827
HTPB_AM1	2.83 ± 0.44	0.87 ± 0.07	15.50 ± 1.62	0.9992
HTPB_AM2	3.14 ± 1.84	0.77 ± 0.26	13.08 ± 0.16	0.9872
HADN	4.83 ± 0.49	0.65 ± 0.05	17.10 ± 1.08	0.9994
HADN_A	3.17 ± 2.79	0.72 ± 0.38	11.67 ± 0.78	0.9708
HADN_M	2.56 ± 0.15	0.84 ± 0.03	13.00 ± 1.33	0.9999

The measured temperatures are reported in Figure 14. The continuum temperature of the non-metalized propellant HADN derives from the emission of soot particles, basically the carbon residues from the binder decomposition. As a rule, the metalized propellants exhibited a rather low temperature (1300 - 1500 K) in comparison with the adiabatic one, as already pointed out for the HTPB series. On the contrary, the soot temperature from the HADN propellant is quite close to the theoretical value (~ 1830 K).
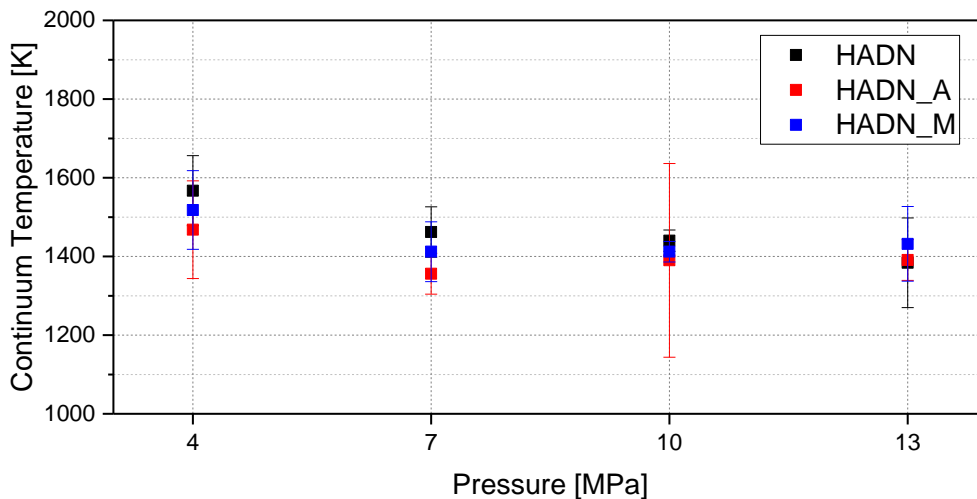
Figure 14: Continuum temperatures from the HADN series.

5. Conclusions and Future Developments

The investigated propellants exhibited a mildly high burning rate, but compliant with the values commonly found in practical applications. The ballistic exponents of all the investigated formulations are the lowest among those known from the open literature (comp. Table *1*), but still too high for the standards adopted in solid propulsion for space launchers. Also a moderate specific impulse (Eq. Vacuum) below 290 s may be a drawback for several applications. An extension of the present work could involve the screening of non-toxic burning rate modifiers, able to reduce the pressure sensitivity. The activation treatment was proven to be effective in modifying the ballistic response of the propellant; nevertheless a dedicated study to tailor the powder reactivity so as to get the desired influence is needed.

The propellants featured a rather weak flame, very susceptible to pressure. It is believed that the burning rate of these formulations is mainly ruled by the decomposition of ADN in the subsurface layer of the propellant, without any strong involvement of the binder [22]. In general very low temperatures were measured if compared with the adiabatic values. In addition to the heat losses typical of a burner, a possible non completion of the gaseous reactions cannot be excluded, given the poor reactivity of the ADN decomposition products.

It is necessary to analyze the temperature profile more in detail, especially in the sub-surface layer. This would be extremely helpful to get a better understanding of both the burning mechanism and the agglomeration phenomena.

Acknowledgments

References

[1] Parr, T. P., and D. Hanson-Parr. 1992. ADN Propellant Diffusion Flame Structure. In: *29th JANNAF Combustion Subcommittee Meeting*. 313–328.

[2] Parr, T. P., and D. Hanson-Parr. 1996. Solid propellant diffusion flame structure. In: *26th Symposium (International) on Combustion*. 1981–1987.

[3] Korobeinichev, O. P., and A. A. Paletsky. 2001. Flame Structure of ADN/HTPB Composite Propellants. *Combustion and Flame*. 127.3:2059–2065.

[4] DeLuca, L. T., I. Palmucci, A. Franzin, V. Weiser, V. Gettwert, N. Wingborg, and M. Sjöblom. 2014. New Energetic Ingredients for Solid Rocket Propulsion. In: 9th International High Energy Materials Conference and Exhibit (HEMCE) ; February 13-15, 2014; Thiruvananthapuram, Kerala, India

[5] de Flon, J., S. Andreasson, M. Liljedahl, C. Oscarson, M. Wanhatalo, and N. Wingborg. 2011. Solid Propellants based on ADN and HTPB. In: *47th AIAA/ASME/ASEE Joint Propulsion Conference & Exhibit*. 6136–6147.

[6] Fujisato, K., H. Habu, H. Shibamoto, X. Yu, A. Miyake, and K. Hori. 2011. Combustion characteristics of ADN-based solid propellants. *Europyro 2011*. S1c-64.

[7] Korobeinichev, O. P., A. A. Paletsky, A. G. Tereschenko, and E. N. Volkov. 2003. Study of Combustion Characteristics of Ammonium Dinitramide/Polycaprolactone Propellants. *Journal of Propulsion and Power*. 19.2:203–212.

[8] Gettwert, V., C. Tagliabue, V. Weiser, and A. Imiolek. 2015. Green Advanced High Energy Propellants for Lauchers (GRAIL) – First results on the Burning Behavior of AN/ADN Propellants. In: *6ᵗʰ European Conference for Aeronautics and Space Sciences (EUCASS)*. 46-(1-14)

[9] Sippel, T. R., S. F. Son, and L. J. Groven. 2013. Altering Reactivity of Aluminum with Selective Inclusion of Polytetrafluoroethylene through Mechanical Activation. *Propellants, Explosives, Pyrotechnics*. 38.2:286–295.

[10] Sippel, T. R., S. F. Son, and L. J. Groven. 2013. Modifying Aluminum Reactivity with Poly(Carbon Monofluoride) via Mechanical Activation. *Propellants, Explosives, Pyrotechnics*. 38.3:321–326.

[11] Dossi, S., C. Paravan, F. Maggi, and L. Galfetti. 2015. Enhancing Micrometric Aluminum Reactivity by Mechanical Activation. In: *51ˢᵗ AIAA/SAE/ASEE Joint Propulsion Conference*. 4221–4235.

[12] Ludwig, C. B., W. Malkmus, J. E. Reardon, J. A. L. Thomson, and R. Goulard. 1973. Handbook of Infrared Radiation from Combustion Gases. *NASA SP-3080*.

[13] Weiser V. and N. Eisenreich. 2005. Fast Emission Spectroscopy for a Better Understanding of Pyrotechnic Combustion Behavior. *Propellants, Explosives, Pyrotechnics*. 30.1: 67–78.

[14] Kelzenberg, S., P. B. Kempa, S. Wurster, M. Herrmann, and T. Fischer. 2014. New Version of the ICT-Thermodynamic Code. In: *45ᵗʰ International Annual Conference of ICT*. 95/1–95/9.

[15] Haynes, W. M. ed. 2017. CRC Handbook of Chemistry and Physics. CRC Press/Taylor & Francis, Boca Raton, FL.

[16] Scudino, S., M. Sakaliyska, K. B. Surreddi, and J. Eckert. 2009. Mechanical alloying and milling of Al-Mg alloys. *Journal of Alloys and Compounds.* 483.1:2–7.

[17] Glotov, O. G. 2000. Condensed Combustion Products of Aluminized Propellants. II. Evolution of Particles with Distance from the Burning Surface. *Combustion, Explosion, and Shock Waves*. 36.4:476–487.

[18] Bucher, P., L. Ernst, F. L. Dryer, and R. Yetter. 2000. Detailed Studies of the Flame Structure of Aluminum Particle Combustion. *Solid Propellant Chemistry, Combustion, and Motor Interior Ballistics, Progress in Astronautics and Aeronautics*. 689–722.

[19] Fabignon, Y., O. Orlandi, J. F. Trubert, D. Lambert, and J. Dupays. 2003. Combustion of Aluminum Particles in Solid Rocket Motors. In: *39ᵗʰ AIAA/ASME/SAE/ASEE Joint Propulsion Conference and Exhibit*. 4807–4817.

[20] Babuk, V. A., V. A. Vasilyev, and M. S. Malakhov. 1999. Condensed Combustion Products at the Burning Surface of Aluminized Solid Propellant. *Journal of Propulsion and Power*. 15.6:783–793.

[21] Babuk, V. A., and A. A. Nizyaev. 2016. The Problem of Formation of the "Hollow" Agglomerates at Burning of Composite Solid Propellants. *Chemical Physics and Mesoscopics*. 18.1:5–16.

[22] V. Weiser, F. Cristilli, V. Gettwert, A. Imiolek, H. Kröber, C. Tagliabue; Investigation of extinguished ADN/HTPB propellants with a special focus on sub-surface reactions; 48th International Annual Conference of ICT; Karlsruhe, Germany; June 27-30, 2017; 122-(1-7)